

Four lepton production in gluon fusion: off-shell Higgs effects in NLO QCD

Massimiliano Grazzini^(a), Stefan Kallweit^(b),
Marius Wiesemann^(c) and Jeong Yeon Yook^(a)

^(a) Physik-Institut, Universität Zürich, 8057 Zürich, Switzerland

^(b) Dipartimento di Fisica, Università degli Studi di Milano-Bicocca and INFN, Sezione di
Milano-Bicocca, 20126, Milan, Italy

^(c) Max-Planck-Institut für Physik, Föhringer Ring 6, 80805 München, Germany

Abstract

We consider the production of four charged leptons in hadron collisions and compute the next-to-leading order (NLO) QCD corrections to the loop-induced gluon fusion contribution by consistently accounting for the Higgs boson signal, its corresponding background and their interference. The contribution from heavy-quark loops is exactly included in the calculation except for the two-loop $gg \rightarrow ZZ \rightarrow 4\ell$ continuum diagrams, for which the unknown heavy-quark effects are approximated through a reweighting procedure. Our calculation is combined with the next-to-next-to-leading order QCD and NLO electroweak corrections to the $q\bar{q} \rightarrow 4\ell$ process, including all partonic channels and consistently accounting for spin correlations and off-shell effects. The computation is implemented in the MATRIX framework and allows us to separately study the Higgs boson signal, the background and the interference contributions, whose knowledge can be used to constrain the Higgs boson width through off-shell measurements. Our state-of-the-art predictions for the invariant-mass distribution of the four leptons are in good agreement with recent ATLAS data.

The observation of a scalar resonance by the ATLAS and CMS experiments [1, 2] at the Large Hadron Collider (LHC) in 2012 marked a milestone towards our understanding of the mechanism of electroweak (EW) symmetry breaking. Studies of its spin, parity and couplings are in good agreement with the hypothesis that the new particle is the Standard Model (SM) Higgs boson. Those studies are mainly focused on on-shell Higgs production. Although for a SM Higgs boson of mass $m_H = 125$ GeV the expected width is $\Gamma_H \sim 4$ MeV, with $\Gamma_H/m_H \sim 3 \times 10^{-5}$, it is well known that off-shell Higgs production has a substantial rate [3]. Furthermore, the interference between Higgs-mediated $gg \rightarrow H \rightarrow VV$ production and continuum $gg \rightarrow VV$ production is strong and destructive in the high invariant-mass region, which is required to preserve unitarity for the scattering amplitudes of massive fermions and gauge bosons.

Off-shell Higgs boson production plays an important role for the determination of the Higgs boson decay width at the LHC. Indeed, the limited resolution of current detectors (~ 1 GeV) prevents a direct measurement of Γ_H . Fortunately, the ratio of the off-shell to the on-shell cross sections can be used [4–7] to set stringent constraints on Γ_H [8–13]. For instance, in a scenario in which the Higgs couplings and width are rescaled from their SM values such that the on-shell cross section remains unchanged [4], the off-shell signal rate would scale with $\Gamma_H/\Gamma_H^{\text{SM}}$, while the interference would scale with $\sqrt{\Gamma_H/\Gamma_H^{\text{SM}}}$. Therefore, in order to constrain Γ_H through off-shell measurements, it is essential to have a precise description of four-lepton production and a separation between the Higgs boson signal, the background and their interference. In the following, we focus on the $H \rightarrow ZZ$ channel and present state-of-art predictions for the three contributions, including the leptonic decays of the Z bosons with off-shell effects and spin correlations.

At leading order (LO) in the strong coupling α_s , continuum ZZ production occurs via quark annihilation. The next-to-leading-order (NLO) QCD prediction for on-shell ZZ production has been known for almost three decades [14, 15] as well as with leptonic decays [16–19]. The NLO electroweak (EW) corrections were first computed for on-shell Z bosons [20–22], and off-shell effects were included in Refs. [23, 24]. In addition, NLO QCD+EW predictions have been calculated for the $2\ell 2\nu$ [25] and $2\ell 2\ell'$ [26] final states. The loop-induced gluon fusion channel enters the computation at $\mathcal{O}(\alpha_s^2)$. Its LO on-shell contribution was first calculated in Refs. [27, 28], followed by the inclusion of leptonic decays [5, 7, 29–35]. The NLO QCD corrections to the loop-induced gluon fusion channel were calculated in Ref. [36–38] for the gluon–gluon (gg) partonic channel using the two-loop amplitudes of Refs. [39, 40], and the full NLO QCD corrections including the quark–gluon (qg) initial states were presented in Ref. [41]. NLO corrections to the Higgs signal–background interference have been considered in Refs. [37, 42]. The full next-to-next-to-leading order (NNLO) QCD corrections (to the quark initiated production) have been obtained both for on-shell Z bosons [43, 44] and for the fully differential leptonic final states [45, 46], using the $q\bar{q} \rightarrow VV'$ two-loop amplitudes of Refs. [47–49]. Recently, also the combination of NNLO QCD and NLO EW predictions has been achieved [50] using MATRIX [51] and OPENLOOPS [52–54]. Finally, by combining the NNLO quark-initiated cross section and the NLO gluon-initiated cross section Ref. [41] presented also approximate N³LO predictions (labelled as nNNLO). Their combination with NLO EW predictions analogous to the results presented in Ref. [55] for W^+W^- production can be achieved with MATRIX as well.

In this Letter, we present new results for four-lepton production at the LHC. We start from the calculation of Ref. [41] and perform a more sophisticated treatment of the heavy-quark mass effects in the two-loop amplitudes of the gg initiated production. As before, both gg and qg partonic channels are considered in the NLO QCD corrections. In addition, we separately study

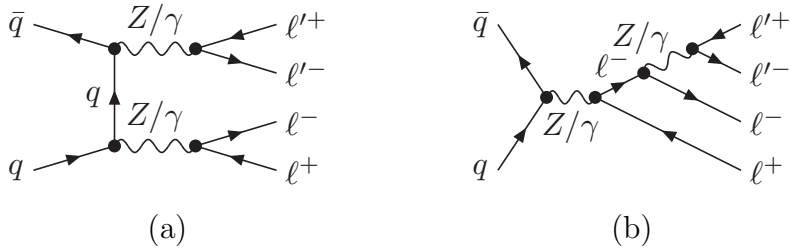


Figure 1: Sample Feynman diagrams for the production of four charged leptons in the quark annihilation channel at LO: (a) t -channel and (b) Drell–Yan-like topologies.

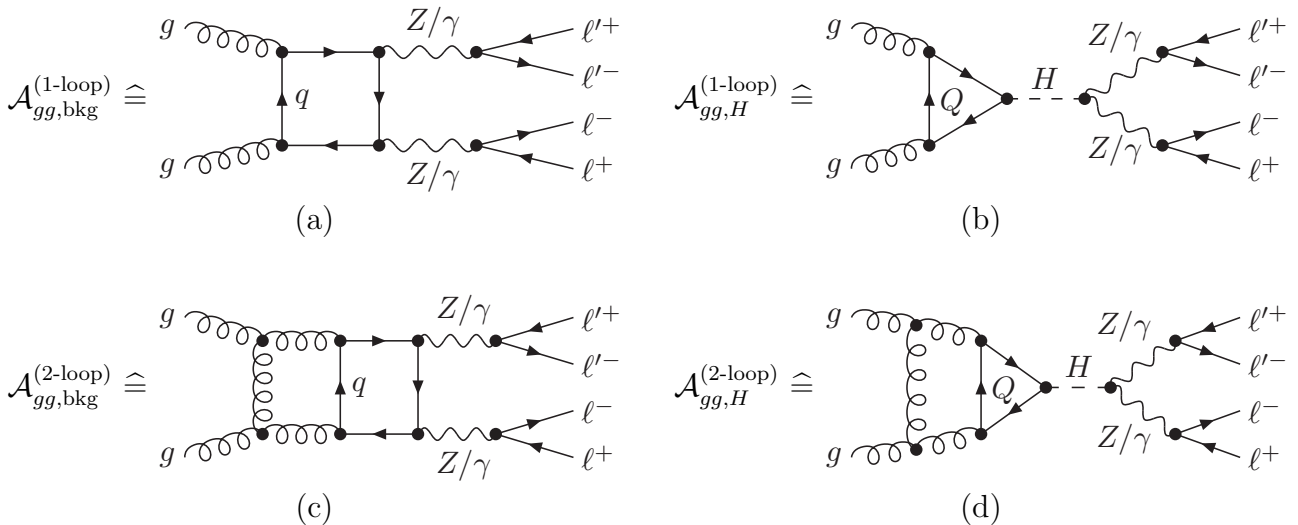


Figure 2: Loop-induced diagrams for the production of four charged leptons in the gluon fusion channel at one-loop level (a,b) and at two-loop level (c,d), separately for the continuum ZZ contributions (a,c) and the Higgs-mediated contributions (b,d). Here, $q \in \{d, u, s, c, b, t\}$ denotes all quarks, whereas $Q \in \{b, t\}$ denotes the quarks treated as massive in this Letter.

the $gg \rightarrow H \rightarrow 4\ell$ signal cross section, the four-lepton continuum background as well as their interference, which are the relevant theoretical ingredients to constrain Γ_H . We also provide state-of-the-art numerical predictions by combining nNNLO QCD and NLO EW corrections, and we compare them with recent ATLAS data at 13 TeV [56].

We consider the four-lepton production process

$$pp \rightarrow \ell^+ \ell^- \ell'^+ \ell'^- + X,$$

both in the same-flavour channel ($\ell' = \ell$) and in the different-flavour channel ($\ell' \neq \ell$), where $\ell, \ell' \in e, \mu$. At the LO, this process is driven by quark annihilation. Representative Born-level diagrams are shown in Figure 1 (a) and (b) for t -channel and Drell–Yan-like topologies, respectively. Starting from NNLO in QCD the contribution from loop-induced diagrams driven by gluon fusion have to be taken into account. Figure 2 (a) and (b) show sample diagrams of the four-lepton continuum and the Higgs-mediated production, respectively. Although those are suppressed by two powers of the strong coupling, their enhancement by the large gluon flux renders them quantitatively important. As a result, the inclusion of NLO corrections to the loop-induced gluon

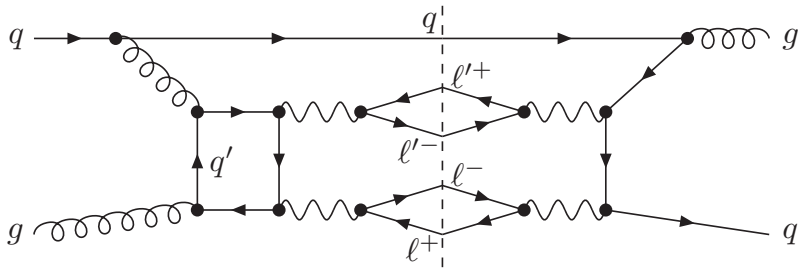


Figure 3: Example of NNLO interference between quark annihilation and loop-induced gluon fusion production mechanisms.

fusion contribution is crucial for precision physics of four-lepton production. Note, however, that the quark annihilation and loop-induced gluon fusion processes cannot be treated as being completely independent. Indeed, they mix already at NNLO in QCD, and Figure 3 illustrates an example. Such contributions have to be included, and the interference renders the distinction between the two production mechanisms cumbersome. As in Refs. [41, 55] we obtain a partial N³LO result, labelled as nNNLO in the following, by combining the NNLO QCD predictions with NLO QCD corrections to the loop-induced gluon fusion contribution, including all partonic channels, but considering only diagrams with purely fermionic loops. Any other N³LO contributions cannot be included consistently at present, and thus they are not considered in our calculation. Nevertheless, those contributions can be expected to be sub-dominant with respect to the corrections we include at nNNLO.

In this Letter, take a few decisive steps in order to advance our calculation in Ref. [41]. In particular, we improve the description of the Higgs signal and signal–background interference by evaluating exactly all the contributions that do not depend on the continuum $gg \rightarrow \ell^+\ell^-\ell'^+\ell'^-$ two-loop helicity amplitude (see below). We perform the calculation by explicitly separating the Higgs boson signal, the four-lepton continuum background, and their interference. Those are the underlying theoretical ingredients the experimental analyses require in order to constrain the Higgs boson width. Finally, as done for W^+W^- production in Ref. [55] we supplement our nNNLO predictions with NLO corrections in the EW coupling expansion, using the implementation presented in Ref. [50].

Our calculation includes the complete dependence on heavy-quark masses in all contributions, but in the two-loop helicity amplitudes of $q\bar{q} \rightarrow \ell^+\ell^-\ell'^+\ell'^-$ and $gg \rightarrow \ell^+\ell^-\ell'^+\ell'^-$, where they are unknown¹. For the quark annihilation process the contribution of closed fermion loops is relatively small, and heavy-quark effects can be safely neglected at two-loop level. By contrast, such effects are important for the loop-induced gluon fusion process, where they enter effectively at LO, i.e. $\mathcal{O}(\alpha_s^2)$, through one-loop diagrams, see Figure 2 (a) and (b). While at one-loop level the full mass dependence is known and included throughout our calculation, at two-loop level, see Figure 2 (c) and (d), the heavy-quark effects for the continuum amplitude in Figure 2 (c) have not yet been computed. As it is well known, the impact of heavy-quark loops is particularly relevant for the Higgs signal–background interference, since in the high-mass region the off-shell Higgs boson decays to longitudinally polarised Z bosons, which in turn have a stronger coupling to heavy quarks. Using an appropriate reweighting procedure the missing heavy-quark contributions can

¹Very recently, the computation of the top-quark contribution to the two-loop on-shell $gg \rightarrow ZZ$ helicity amplitudes has been reported [57, 58].

be approximated. In the following, we discuss in detail the approach used in Ref. [55] and the improvement pursued here. To this end, we define the finite part (in the hard scheme [59]) of the one-loop and two-loop amplitudes $\mathcal{A}_{gg,\text{bkg}}^{(1\text{-loop})}$, $\mathcal{A}_{gg,H}^{(1\text{-loop})}$ and $\mathcal{A}_{gg,\text{bkg}}^{(2\text{-loop})}$, $\mathcal{A}_{gg,H}^{(2\text{-loop})}$ separately for the four-lepton continuum background and the Higgs-mediated contribution, as indicated in Figure 2 with one sample diagram for each amplitude. The α_S expansion of the full $gg \rightarrow \ell^+ \ell^- \ell'^+ \ell'^-$ amplitude and its square can then be written as

$$\mathcal{A}_{gg \rightarrow 4\ell} = \alpha_S \left(\mathcal{A}_{gg,\text{bkg}}^{(1\text{-loop})} + \mathcal{A}_{gg,H}^{(1\text{-loop})} \right) + \alpha_S^2 \left(\mathcal{A}_{gg,\text{bkg}}^{(2\text{-loop})} + \mathcal{A}_{gg,H}^{(2\text{-loop})} \right) + \mathcal{O}(\alpha_S^3), \quad (1)$$

$$\begin{aligned} |\mathcal{A}_{gg \rightarrow 4\ell}|^2 &= \alpha_S^2 \left(\mathcal{A}_{gg,\text{bkg}}^{(1\text{-loop})} + \mathcal{A}_{gg,H}^{(1\text{-loop})} \right)^* \left(\mathcal{A}_{gg,\text{bkg}}^{(1\text{-loop})} + \mathcal{A}_{gg,H}^{(1\text{-loop})} \right) \\ &\quad + \alpha_S^3 \times 2 \text{Re} \left[\left(\mathcal{A}_{gg,\text{bkg}}^{(1\text{-loop})} + \mathcal{A}_{gg,H}^{(1\text{-loop})} \right)^* \left(\mathcal{A}_{gg,\text{bkg}}^{(2\text{-loop})} + \mathcal{A}_{gg,H}^{(2\text{-loop})} \right) \right] + \mathcal{O}(\alpha_S^4). \end{aligned} \quad (2)$$

In fact, each of the amplitudes in Eq. (1) is known with its full heavy-quark mass dependence, except for $\mathcal{A}_{gg,\text{bkg}}^{(2\text{-loop})}$, which is known only for massless quark loops. In Ref. [55] we have computed the entire α_S^3 contribution to the squared amplitude in the massless approximation, reweighted with the full mass dependence at one-loop,

$$\begin{aligned} &\left(\mathcal{A}_{gg,\text{bkg}}^{(1\text{-loop})} + \mathcal{A}_{gg,H}^{(1\text{-loop})} \right)^* \left(\mathcal{A}_{gg,\text{bkg}}^{(2\text{-loop})} + \mathcal{A}_{gg,H}^{(2\text{-loop})} \right) \\ &\approx \frac{\left(\mathcal{A}_{gg,\text{bkg}}^{(1\text{-loop,massless})} + \mathcal{A}_{gg,H}^{(1\text{-loop,massless})} \right)^* \left(\mathcal{A}_{gg,\text{bkg}}^{(2\text{-loop,massless})} + \mathcal{A}_{gg,H}^{(2\text{-loop,massless})} \right)}{\left(\mathcal{A}_{gg,\text{bkg}}^{(1\text{-loop,massless})} + \mathcal{A}_{gg,H}^{(1\text{-loop,massless})} \right)^* \left(\mathcal{A}_{gg,\text{bkg}}^{(1\text{-loop,massless})} + \mathcal{A}_{gg,H}^{(1\text{-loop,massless})} \right)} \\ &\quad \times \left(\mathcal{A}_{gg,\text{bkg}}^{(1\text{-loop})} + \mathcal{A}_{gg,H}^{(1\text{-loop})} \right)^* \left(\mathcal{A}_{gg,\text{bkg}}^{(1\text{-loop})} + \mathcal{A}_{gg,H}^{(1\text{-loop})} \right), \end{aligned} \quad (3)$$

where $\mathcal{A}_{gg,H}^{(1\text{-loop,massless})} = \mathcal{A}_{gg,H}^{(2\text{-loop,massless})} = 0$. However, also the two-loop Higgs form factor relevant to compute $\mathcal{A}_{gg,H}^{(2\text{-loop})}$ is known including the full heavy-quark mass effects [60–63]. In particular, in the new implementation we use the explicit expression of Ref. [64] and combine it with the $gg \rightarrow H \rightarrow \ell^+ \ell^- \ell'^+ \ell'^-$ one-loop amplitude, taking care of the correct complex phases in the amplitude definition, to obtain the full result for $\mathcal{A}_{gg,H}^{(2\text{-loop})}$. In a second step, we apply a judicious reweighting procedure, using the full one-loop amplitudes to approximate the mass effects in all contributions interfered with $\mathcal{A}_{gg,\text{bkg}}^{(2\text{-loop})}$,

$$\begin{aligned} &\left(\mathcal{A}_{gg,\text{bkg}}^{(1\text{-loop})} + \mathcal{A}_{gg,H}^{(1\text{-loop})} \right)^* \mathcal{A}_{gg,\text{bkg}}^{(2\text{-loop})} \\ &\approx \frac{\left(\mathcal{A}_{gg,\text{bkg}}^{(1\text{-loop})} + \mathcal{A}_{gg,H}^{(1\text{-loop})} \right)^* \mathcal{A}_{gg,\text{bkg}}^{(2\text{-loop,massless})}}{\left(\mathcal{A}_{gg,\text{bkg}}^{(1\text{-loop})} + \mathcal{A}_{gg,H}^{(1\text{-loop})} \right)^* \mathcal{A}_{gg,\text{bkg}}^{(1\text{-loop,massless})}} \times \left(\mathcal{A}_{gg,\text{bkg}}^{(1\text{-loop})} + \mathcal{A}_{gg,H}^{(1\text{-loop})} \right)^* \mathcal{A}_{gg,\text{bkg}}^{(1\text{-loop})}. \end{aligned} \quad (4)$$

Note that this reweighting procedure is implemented at the level of the squared/interfered amplitudes, since this amounts to simply multiplying complex numbers, rather than at the amplitude level before summing over helicities, which would be more involved. However, Eq. (4) effectively corrects only for the missing quark-mass effects in $\mathcal{A}_{gg,\text{bkg}}^{(2\text{-loop})}$. It is clear that with this approximation we obtain a much better treatment of the heavy-quark effects, especially of the Higgs contributions, than using Eq. (3). In fact, with the new implementation the Higgs signal does not include any approximation. One part of the interference contribution is complete as well, while the other part includes the mass effects of the one-loop correction. Only the background contribution is

treated essentially in the same approximation as in Ref. [55]. However, given that also the NNLO $q\bar{q}$ cross section is part of the background to the Higgs signal, this approximation is subleading. In particular, the Higgs interference contribution in our approach is a new result including all contributions known to date, which will be useful for constraining the Higgs width.

Our calculation is performed within the MATRIX framework [51]. With MATRIX, NNLO QCD predictions can be obtained for various colour-singlet processes at hadron colliders [43, 45, 46, 65–71].² The core of MATRIX is the Monte Carlo program MUNICH [80] which contains a fully automated implementation of the dipole subtraction method [81, 82] and an efficient phase space integration. NLO corrections can be obtained using either dipole subtraction or q_T subtraction [83], which provides a self-consistency check for our results. All tree-level and one-loop amplitudes can be evaluated with either OPENLOOPS 2 [52–54] or RECOLA 2 [84, 85], and the corresponding numerical results are in full agreement. In case of OPENLOOPS, we use dedicated squared amplitudes to separate the Higgs signal, background and interference contributions in the gluon fusion channel. In case of RECOLA, we exploit the SM_FERM_YUK model to select the order of the top and bottom Yukawa couplings. With this model, our RECOLA 2 implementation allows us to separate the Higgs signal and background at the level of helicity amplitudes. Also in the calculation of the two-loop corrections, following Eq. (1) and using the approximation in Eq. (4), we exploit RECOLA 2 with the SM_FERM_YUK model to select the relevant one-loop helicity amplitudes $\mathcal{A}_{gg,\text{bkg}}^{(1\text{-loop})}$ and $\mathcal{A}_{gg,H}^{(1\text{-loop})}$. For the two-loop amplitudes, we exploit the calculation of the massless helicity amplitudes of Ref. [40] that are implemented in VVAMP [86] to obtain $\mathcal{A}_{gg,\text{bkg}}^{(2\text{-loop,massless})}$, and we apply the two-loop Higgs form factor including the full heavy-quark mass effects of Ref. [64] to the one-loop helicity amplitude $\mathcal{A}_{gg,H}^{(1\text{-loop})}$ from RECOLA 2 in order to compute $\mathcal{A}_{gg,H}^{(2\text{-loop})}$. To obtain the NNLO corrections to the quark-initiated process we exploit the general implementation of the q_T subtraction formalism [83] within MATRIX and rely on the two-loop $q\bar{q} \rightarrow 4\ell$ helicity amplitudes of Ref. [49] that are also provided by VVAMP [86].

Our implementation of NLO QCD corrections to the loop-induced gluon fusion production with separation of Higgs signal, background and interference has been validated by comparing fiducial and differential cross sections to the results of Ref. [37]. Ref. [37] presents an NLO calculation of the Higgs signal, the continuum ZZ background and their interference, considering the $e^+e^-\mu^+\mu^-$ channel. The calculation of Ref. [37] is limited to the gg partonic channel and includes the top-quark loops in the two-loop $gg \rightarrow ZZ$ amplitude through a large- m_t expansion. To the purpose of our comparison we exactly reproduce the setup of Ref. [37], except for the treatment of the bottom quarks, which Ref. [37] considers as massless in the background amplitudes and as massive in the Higgs-mediated amplitudes. MATRIX, on the other hand, treats bottom quarks as either massless or massive particles throughout the calculation in a consistent manner. At LO we find complete agreement with the results of Ref. [37], and we have independently checked our results with the parton level Monte Carlo program MCFM [18, 87, 88]. At NLO we are able to reproduce the results of Eq. (4) of Ref. [37] to better than 1% percent. We also find reasonably good agreement with the four-lepton invariant mass distributions reported in Fig. 6 of Ref. [37]. Considering the different treatment of the bottom quarks, and the different approximation used for the top-quark contributions, we regard this agreement fully satisfactory.

We now present predictions for $pp \rightarrow \ell^+\ell^-\ell'^+\ell'^-$ production at $\sqrt{s} = 13$ TeV. The two lepton pairs

²It was also used in the NNLO+NNLL computation of Ref. [72], in the NNLO+N³LL computations of Ref. [73, 74], and in the NNLO+PS computations of Refs. [75–79].

definition of the fiducial volume for $pp \rightarrow 4\ell + X$
muon selection with $p_{T,\mu} > 5 \text{ GeV}$ and $ \eta_\mu < 2.7$
electron selection with $p_{T,e} > 7 \text{ GeV}$ and $ \eta_e < 2.47$
$p_{T,\ell_1} > 20 \text{ GeV}$, $p_{T,\ell_2} > 15 \text{ GeV}$ and $p_{T,\ell_3} > 10 \text{ GeV}$ for leading three leptons
$50 \text{ GeV} < m_{12} < 106 \text{ GeV}$ and $f(m_{4\ell}) < m_{34} < 115 \text{ GeV}$
$\Delta R_{\ell_i \ell_j} > 0.1(0.2)$ for same (opposite) flavour leptons
$m_{\ell_i \ell_j} > 5 \text{ GeV}$ for all same-flavour opposite-sign pairs
$70 \text{ GeV} < m_{4\ell} < 1200 \text{ GeV}$

Table 1: Fiducial phase-space definitions of the ATLAS ZZ measurements at $\sqrt{s} = 13 \text{ TeV}$ [56].

$\ell^+ \ell^-$ and $\ell'^+ \ell'^-$ may have the same ($\ell = \ell'$) or different ($\ell \neq \ell'$) flavours with $\ell, \ell' \in \{e, \mu\}$. We use the selection cuts adopted in the ATLAS analysis of Ref. [56], summarized in Table 1. The three leading leptons must have transverse momenta p_{T,ℓ_1} , p_{T,ℓ_2} and p_{T,ℓ_3} larger than 20, 15, and 10 GeV, respectively. The fourth lepton is required to have $p_T > 7(5)$ GeV for electrons (muons). The electron and muon pseudorapidities must fulfil $|\eta_e| < 2.47$ and $|\eta_\mu| < 2.7$, respectively. For each event, the lepton pair with an invariant mass m_{12} closest to the Z boson mass is required to have m_{12} in the range $50 \text{ GeV} < m_{12} < 106 \text{ GeV}$. The remaining pair is referred to as the secondary pair, with mass m_{34} , and it must fulfil $f(m_{4\ell}) < m_{34} < 115 \text{ GeV}$, where the function $f(m_{4\ell})$ is [56]

$$f(m_{4\ell}) = \begin{cases} 5 \text{ GeV}, & \text{for } m_{4\ell} < 100 \text{ GeV} \\ 5 \text{ GeV} + 0.7 \times (m_{4\ell} - 100 \text{ GeV}), & \text{for } 100 \text{ GeV} < m_{4\ell} < 110 \text{ GeV} \\ 12 \text{ GeV}, & \text{for } 110 \text{ GeV} < m_{4\ell} < 140 \text{ GeV} \\ 12 \text{ GeV} + 0.76 \times (m_{4\ell} - 140 \text{ GeV}), & \text{for } 140 \text{ GeV} < m_{4\ell} < 190 \text{ GeV} \\ 50 \text{ GeV}, & \text{for } m_{4\ell} > 190 \text{ GeV} \end{cases} \quad (5)$$

This selection strategy is tailored to preserve a good acceptance for low $m_{4\ell}$ values, but to suppress events with leptonic τ decays at higher $m_{4\ell}$. Leptons with different (same) flavours are separated by $\Delta R > 0.2(0.1)$. The invariant mass of each same-flavour opposite-sign lepton pair is required to be larger than 5 GeV. Finally, an invariant-mass range of $70 \text{ GeV} < m_{4\ell} < 1200 \text{ GeV}$ is imposed on the four-lepton system.

For the electroweak parameters we use the G_μ scheme and set $\alpha = \sqrt{2} G_\mu m_W^2 (1 - m_W^2/m_Z^2)/\pi$. The EW mixing angle is computed as $\cos \theta_W^2 = (m_W^2 - i\Gamma_W m_W)/(m_Z^2 - i\Gamma_Z m_Z)$, and the complex-mass scheme [89] is used. The EW inputs are set to the PDG [90] values: $G_F = 1.16639 \times 10^{-5} \text{ GeV}^{-2}$, $m_W = 80.385 \text{ GeV}$, $\Gamma_W = 2.0854 \text{ GeV}$, $m_Z = 91.1876 \text{ GeV}$, $\Gamma_Z = 2.4952 \text{ GeV}$, $m_H = 125 \text{ GeV}$, and $\Gamma_H = 0.00407$. The on-shell top-quark and bottom-quark masses are set to $m_t = 173.2 \text{ GeV}$ and $m_b = 4.5 \text{ GeV}$, respectively, with $\Gamma_t = 1.44262 \text{ GeV}$. Apart from the virtual two-loop contributions, the full dependence on massive top and bottom quarks is taken into account everywhere in the computation, and the four-flavour scheme with $N_f = 4$ massless quark flavours is used. We employ the corresponding NNPDF31_nnlo_as_0118_luxqed_nf_4 [91] PDF set with $\alpha_S(m_Z) = 0.118$ at LO, NLO, and NNLO. The renormalization and factorization scales are set dynamically to half of the four-lepton invariant mass, $\mu_R = \mu_F = m_{4\ell}/2$, and scale uncertainties are estimated through customary 7-point scale variations with the constraint $0.5 \leq \mu_R/\mu_F \leq 2$.

$\sqrt{s} = 13 \text{ TeV}$	$\sigma \text{ [fb]}$	$\sigma/\sigma_{\text{NLO}} - 1$
LO	36.848(1) $\begin{smallmatrix} +7.1\% \\ -8.1\% \end{smallmatrix}$	-24.8%
NLO	48.990(2) $\begin{smallmatrix} +3.1\% \\ -2.9\% \end{smallmatrix}$	—
$q\bar{q}$ NNLO	52.07(4) $\begin{smallmatrix} +1.4\% \\ -1.4\% \end{smallmatrix}$	+6.3%
	$\sigma \text{ [fb]}$	$\sigma/\sigma_{\text{ggLO}} - 1$
gg LO	4.2967(3) $\begin{smallmatrix} +25.6\% \\ -18.4\% \end{smallmatrix}$	—
gg NLO	7.80(2) $\begin{smallmatrix} +17.1\% \\ -13.9\% \end{smallmatrix}$	+81.5%
	$\sigma \text{ [fb]}$	$\sigma/\sigma_{\text{NLO}} - 1$
NNLO	56.37(4) $\begin{smallmatrix} +3.2\% \\ -2.7\% \end{smallmatrix}$	+15.1%
nNNLO	59.87(4) $\begin{smallmatrix} +3.4\% \\ -3.1\% \end{smallmatrix}$	+22.2%
nNNLO _{bkg}	58.37(4) $\begin{smallmatrix} +2.8\% \\ -2.6\% \end{smallmatrix}$	+19.1%
	$\sigma \text{ [fb]}$	$\sigma/\sigma_{\text{nNNLO}} - 1$
nNNLO _{EW}	56.49(4) $\begin{smallmatrix} +3.5\% \\ -3.1\% \end{smallmatrix}$	-5.6%

Table 2: Fiducial cross sections in the phase space volume defined in Ref. [56] and summarized in Table 1 at different perturbative orders. Statistical uncertainties for (n)NNLO results include the uncertainties due the r_{cut} extrapolation in q_T subtraction [51].

We start the presentation of our results in Table 2 with the fiducial cross sections corresponding to the selection cuts in Table 1. We use the following notation: $q\bar{q}$ NNLO refers to the NNLO result for the $q\bar{q}$ -initiated process, see Figure 1, without the loop-induced gluon fusion contribution; gg LO and gg NLO refer to the loop-induced gluon fusion contribution, see Figure 2, at $\mathcal{O}(\alpha_s^2)$ and up to $\mathcal{O}(\alpha_s^3)$, respectively; nNNLO is the sum of $q\bar{q}$ NNLO and gg NLO; nNNLO_{bkg} is the corresponding cross section including only the continuum background without Higgs contributions, whereas all other cross sections include resonant and non-resonant Higgs diagrams, where applicable; nNNLO_{EW} is our best prediction for the fiducial cross section. It is obtained as in Ref. [55] for WW production by including EW corrections (to the $q\bar{q}$ channel) in a factorised approach [50].

With respect to the NLO cross section, the NNLO corrections in the $q\bar{q}$ channel amount to +6.3% while the full NNLO corrections amount to +15.1%.³ Therefore, the loop-induced gluon fusion process contributes 58% of the NNLO correction. This is in line with previous computations [41, 43, 45, 46, 51]. The NLO corrections to the loop-induced contribution are huge, increasing gg LO by +81.2%, which is even slightly higher than the +70.8% correction found with the setup considered in Ref. [41], where the Higgs resonance region is excluded from the fiducial volume.

³Note that the NLO and NNLO K -factors in the $q\bar{q}$ channel are smaller here than in Ref. [41] essentially due to the different choices of the PDFs at LO and NLO.

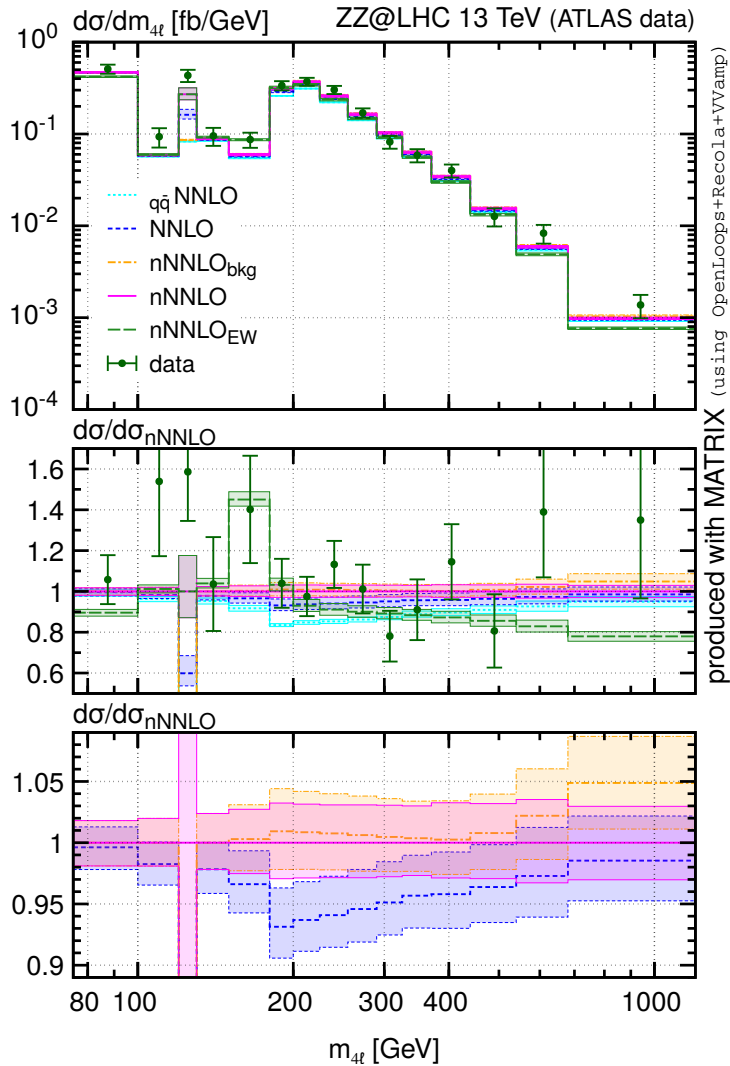


Figure 4: Invariant-mass distribution of the four leptons in the phase space volume defined in Ref. [56] and summarized in Table 1, compared to data from Ref. [56].

This confirms once more that those corrections depend on the fiducial cuts under consideration and cannot be included through global rescaling factors. The $n\text{NNLO}$ result is +22.2% higher than the NLO cross section, +6.2% higher than the NNLO cross section, and +2.6% higher than the $n\text{NNLO}_{\text{bkg}}$ Higgs background prediction. This means that the Higgs boson has a positive contribution of 2.6% at $n\text{NNLO}$. Finally, the EW corrections lead to a reduction of the cross section by -5.6% , which cancels almost exactly the contribution from the $gg\text{NLO}$ corrections so that the $n\text{NNLO}_{\text{EW}}$ prediction is only two permille above the NNLO cross section. However, while such cancellation may occur at the level of the integrated cross section with a given set of fiducial cuts, $gg\text{NLO}$ and NLO EW corrections have an effect in different regions of phase space and therefore do not compensate each other in differential distributions.

In Figure 4 we show different predictions for the invariant-mass distribution of the four leptons and compare them against ATLAS data from Ref. [56] (green dots with experimental error bars). In particular, we show $q\bar{q}\text{NNLO}$ (light blue, dotted), NNLO (blue, dashed), $n\text{NNLO}$ with (magenta,

solid) and without (orange, dash-dotted) Higgs contributions, and finally nNNLO predictions including EW corrections (green, long-dashed). The top panel shows the absolute distributions, while the lower two panels show predictions and data normalised to the nNNLO result. The agreement between theory and data is quite good. Unfortunately, the experimental uncertainties are still too large to clearly resolve the differences between the various theoretical predictions. In particular, despite clear differences of the nNNLO and nNNLO_{EW} predictions at high invariant mass and in the bin below the $2m_Z$ threshold, both predictions show a similar level of agreement to data, given the rather large experimental uncertainties. Nevertheless, one can make the following two interesting observations: First, in that bin below the $2m_Z$ threshold, where large QED corrections are indeed expected, the nNNLO_{EW} prediction is in better agreement with the data point. Second, in the tail of the invariant-mass distribution, where EW corrections have a large impact, data actually seem to be quite high and more consistent with the nNNLO result. Although this comparison has to be taken with caution due to the large experimental errors in that region, this (small) $\sim 1.5\sigma$ excess over nNNLO_{EW} in the last two bins is an important demonstration of why EW corrections are so crucial: If with decreasing experimental uncertainties one were to consider only the QCD prediction in such phase space region, an excess of the data over the actual SM prediction including EW corrections might go unnoticed.

We also find that in the region around $m_{4\ell} \sim 200$ GeV the NNLO prediction in the $q\bar{q}$ channel is almost 20% smaller than the nNNLO result, which shows that also the loop-induced gg channel yields a substantial contribution to the cross section. Indeed, the analysis of Ref. [56] extracts a signal strength of the loop-induced gluon fusion contribution of $\mu_{gg} = 1.3 \pm 0.5$. Note that the gg contribution becomes even larger in the bin around $m_{4\ell} = 125$ GeV due to the Higgs resonance. In that bin $q\bar{q}$ NNLO and nNNLO_{bkg} predictions are way below data, since they do not include resonant Higgs contributions. Also the NNLO prediction is quite low, since it misses the large NLO corrections to Higgs production. However, one should bear in mind that also the full nNNLO prediction misses the relatively large higher-order corrections to on-shell Higgs production beyond NLO (see Ref. [92] and references therein).

In the bottom panel we increase the resolution of the relative differences to nNNLO for a subset of the QCD predictions. Comparing the NNLO and nNNLO results we see that their uncertainty bands overlap almost everywhere. The largest effect of nNNLO corrections is in the region $m_{4\ell} \sim 200$ GeV where the difference with NNLO is about 7%. We also notice that the Higgs background prediction departs from the full result as $m_{4\ell}$ increases, where it becomes larger. The effect is about +5% in the last $m_{4\ell}$ bin. This means that in this region the relative impact of the Higgs contribution is negative and becomes increasingly large, which is caused by the Higgs signal-background interference. In the following, we will investigate in more detail the relative effects when separating Higgs signal, background and interference contributions.

We now continue our presentation of phenomenological results by studying the theoretical ingredients used in Higgs off-shell studies to constrain Γ_H at the LHC. The relevant quantity is the ratio of the off-shell to the on-shell Higgs cross section [12, 13]. To this end, we report in Table 3 various contributions to the fiducial cross section in the off-shell region with $m_{4\ell} > 200$ GeV (left) and in the Higgs signal region $120 \text{ GeV} < m_{4\ell} < 130 \text{ GeV}$ (right). Besides the notation already introduced in the discussion of Table 2, we use the abbreviations “sig”, “bkg”, and “intf” to separate the 4ℓ Higgs signal contribution, the 4ℓ continuum background contribution, and their interference, respectively. We recall that this separation is needed when constraining the Higgs width at the LHC [12, 13]. In particular, in the scenario proposed in Ref. [4] the Higgs couplings and width are

$\sqrt{s} = 13 \text{ TeV}$	$m_{4\ell} > 200 \text{ GeV}$			$120 < m_{4\ell} < 130 \text{ GeV}$		
	$\sigma \text{ (fb)}$	$\sigma/\sigma_{ggLO} - 1$		$\sigma \text{ (fb)}$	$\sigma/\sigma_{ggLO} - 1$	
$ggLO$	2.73726(28)	+25.32% -18.57%	—	0.78952(12)	+28.48% -19.83%	—
$ggNLO$	4.5790(53)	+14.24% -12.46%	+67.3%	1.8745(87)	+24.88% -18.02%	+137.4%
	$\sigma \text{ (fb)}$	$\sigma/\sigma_{ggLO}^{\text{bkg}} - 1$		$\sigma \text{ (fb)}$	$\sigma/\sigma_{ggLO}^{\text{bkg}} - 1$	
$ggLO_{\text{bkg}}$	2.89117(27)	+25.38% -18.61%	—	0.018466(31)	+28.47% -19.83%	—
$ggNLO_{\text{bkg}}$	4.8615(33)	+14.32% -12.48%	+68.2%	0.0315(32)	+16.61% -13.96%	+70.6%
	$\sigma \text{ (fb)}$	$\sigma/\sigma_{ggLO}^{\text{intf}} - 1$		$\sigma \text{ (fb)}$	$\sigma/\sigma_{ggLO}^{\text{intf}} - 1$	
$ggLO_{\text{intf}}$	-0.333378(29)	-19.76% +26.97%	—	0.000215(10)	+28.55% -19.86%	—
$ggNLO_{\text{intf}}$	-0.6174(42)	-14.35% +17.18%	+85.2%	0.00035(33)	+13.46% -12.40%	+64.3%
	$\sigma \text{ (fb)}$	$\sigma/\sigma_{ggLO}^{\text{sig}} - 1$		$\sigma \text{ (fb)}$	$\sigma/\sigma_{ggLO}^{\text{sig}} - 1$	
$ggLO_{\text{sig}}$	0.180110(16)	+27.50% -20.19%	—	0.770793(29)	+28.48% -19.83%	—
$ggNLO_{\text{sig}}$	0.33555(14)	+17.15% -14.35%	+86.3%	1.8426(81)	+25.03% -18.09%	+139.1%
	$\sigma \text{ (fb)}$	$\sigma/\sigma_{\text{NLO}} - 1$		$\sigma \text{ (fb)}$	$\sigma/\sigma_{\text{NLO}} - 1$	
LO	21.37744(43)	+4.15% -5.08%	-23.7%	0.633439(77)	+11.31% -12.46%	-19.8%
NLO	28.02236(77)	+2.80% -2.31%	—	0.78944(16)	+2.84% -4.64%	—
$q\bar{q}NNLO$	29.887(12)	+1.45% -1.41%	+6.7%	0.8296(26)	+1.15% -1.22%	+5.1%
NNLO	32.625(12)	+3.44% -2.83%	+16.4%	1.6191(26)	+14.48% -10.30%	+105.1%
nNNLO	34.466(13)	+3.13% -2.87%	+23.0%	2.7041(91)	+17.60% -12.87%	+242.5%
nNNLO _{EW}	31.052(12)	+3.31% -3.02%	+10.8%	2.7043(91)	+17.60% -12.87%	+242.6%

Table 3: Integrated cross sections in the four-lepton invariant-mass ranges $m_{4\ell} > 200 \text{ GeV}$ and $120 < m_{4\ell} < 130 \text{ GeV}$ in the fiducial phase space defined in Ref. [56], at different perturbative orders. The Higgs signal (sig), background (bkg), and interference (intf) contributions in the loop-induced gg channel are stated separately.

rescaled from their SM values such that the on-shell cross section remains unchanged. In this case, the off-shell Higgs rate needs to be evaluated by adding the Higgs signal contribution rescaled by $\Gamma_H/\Gamma_H^{\text{SM}}$ and the Higgs interference contribution rescaled by $\sqrt{\Gamma_H/\Gamma_H^{\text{SM}}}$. Accurate predictions of the separate contributions of the Higgs boson signal, the background and their interference are therefore indispensable for such analyses.

We start our discussion from the region $m_{4\ell} > 200$ GeV. We see that in this region the interference is negative, as expected from unitarity arguments. Therefore, the gluon fusion cross section is smaller than the sum of the signal and background cross sections by about 11% both at LO and at NLO. In particular, the interference is almost twice as large as the signal in absolute value, and its size is about 12% compared to the background, which in turn is only about 17% of the NNLO result in the $q\bar{q}$ channel. The large cancellations between signal and interference render the separation of the off-shell Higgs cross section from the background difficult. We note that, as argued in early off-shell studies (see e.g. Ref. [93]), the NLO K -factor for the interference is very close to the geometrical average of the K -factors for signal and background. However, we stress that this conclusion is strongly dependent on the fiducial cuts and setup under consideration.

We now continue our discussion of Table 3 with the region $120 \text{ GeV} < m_{4\ell} < 130 \text{ GeV}$. As expected, the Higgs signal cross section is by far dominant due to resonant Higgs contributions, being about 60 times larger than the gluon fusion background. The interference is positive, but about two orders of magnitude smaller than the background. It is worth noticing that the size of the NLO corrections for signal, background and interference is relatively similar when the Higgs boson is off-shell, whereas in the region where the Higgs boson can become on-shell the NLO K -factor of the signal contribution is significantly larger than that of background and interference.

In Figure 5 we study the behaviour of the signal, background and interference contributions to the invariant-mass distribution in the loop-induced gluon fusion channel. We use the same invariant-mass range and binning as considered in the ATLAS analysis [56]. In Figure 5(a) we show the full result at LO (turquoise, long-dashed) and NLO (magenta, solid). For comparison, also the signal (blue, dashed), the background (red, dotted), and the modulus of the interference contribution (purple, dash-dotted) are shown at NLO in the main frame. The separate LO and NLO results for the signal, the background and the interference are presented in Figure 5(b), (c), and (d), respectively. In the lower panels we study the different behaviour of the NLO K -factors, i.e. the ratios of the NLO to the LO predictions.

For the signal contribution we clearly see the peak at $m_{4\ell} = 125$ GeV from the Higgs resonance, and then the cross section quickly drops and increases again at the $2m_Z$ threshold, remaining roughly constant up about 400 GeV where it starts to decrease again. Above 400 GeV the signal and the interference are of the same order, while for $200 \lesssim m_{4\ell} \lesssim 400$ GeV the absolute value of the negative interference contribution is even larger. These features are well known [3, 94]: the decrease of the signal cross section due to the off-shell Higgs boson propagator is compensated by the $|\mathcal{A}|^2 \sim m_{4\ell}^4$ increase of the decay amplitude, thereby leading to the plateau observed in Figure 5(b). For the signal the impact of the NLO corrections is about +170% at small invariant masses, and it slowly decreases as $m_{4\ell}$ increases, being about +60% in the high-mass region. The background distribution has a broad maximum for $m_{4\ell} \gtrsim 2m_Z$ due to the ZZ resonance, while the impact of NLO corrections is more uniform, ranging from about 100% in the second bin to 60% in the high- $m_{4\ell}$ region. The interference is negative and peaked at $m_{4\ell} \sim 200$ GeV, but it changes sign in the Higgs signal region. In the region $m_{4\ell} \sim 200$ GeV the NLO corrections to

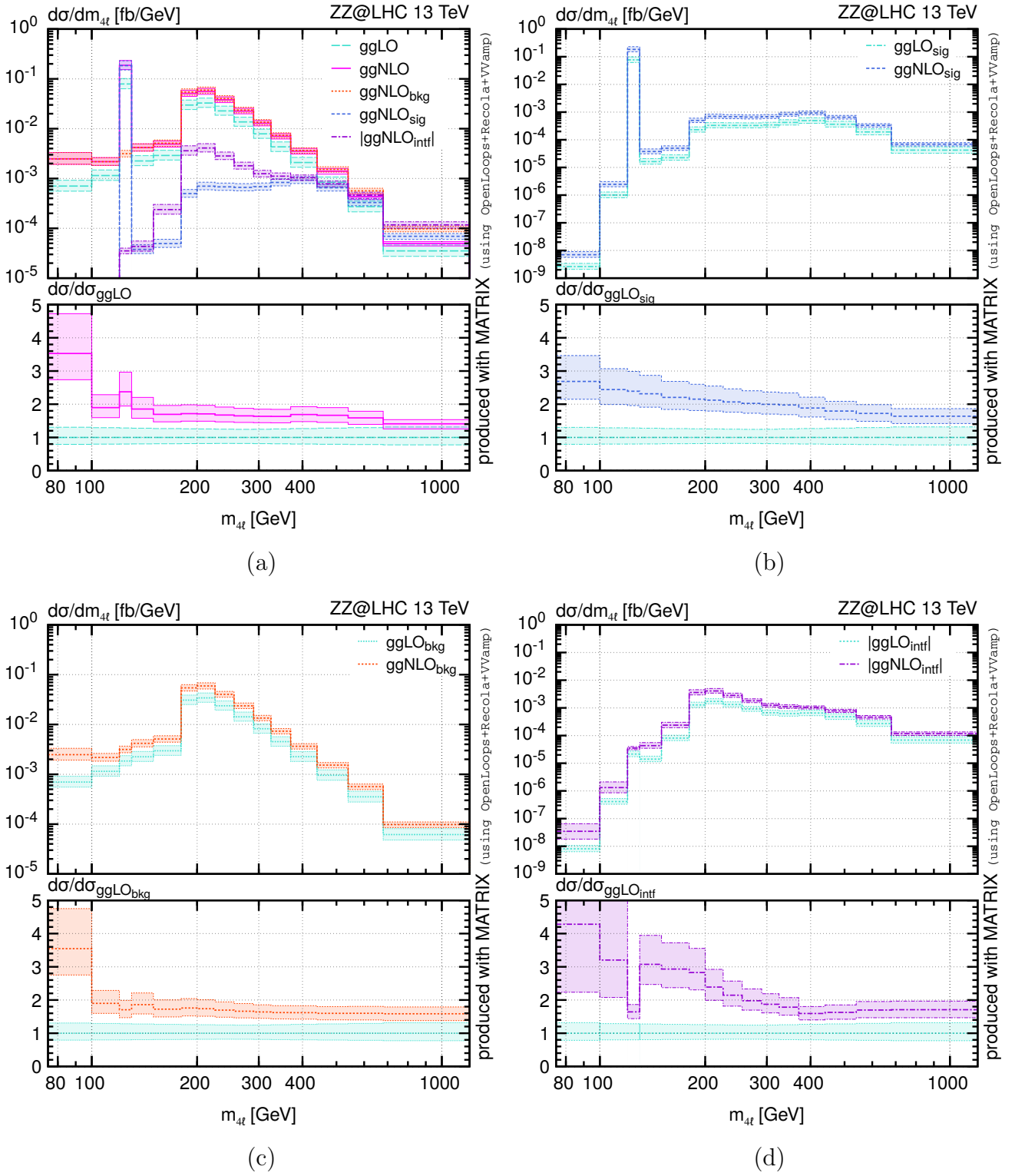


Figure 5: Four-lepton invariant mass distribution for the loop-induced gg channel with the phase space definition of Ref. [56]. We show the full result (a), as well as the contributions of the Higgs signal (b), background (c) and interference (d) separately.

the interference are very large (about +150%), and they are larger than for the signal and the background, decreasing to about 70% at large values of $m_{4\ell}$.

In conclusion, in all cases radiative corrections have the effect of increasing the absolute size of the individual contributions. However, the relative size of the corrections for the individual contributions is quite different, especially at small $m_{4\ell}$ values, and the full result is a combination of all of those effects. Only at large invariant masses ($m_{4\ell} \gtrsim 400$ GeV) the relative size of the corrections becomes similar for signal, background and interference. It is therefore difficult to make a direct connection between the QCD corrections beyond NLO for the signal, which are known to be relatively large (see Ref. [92] and references therein), and the other contributions, where they are not known. Nevertheless, the NLO corrections in the off-shell region are not that different among the three contributions, and the QCD effects beyond NLO are expected to be significant. Therefore, in order to approximately take higher-order corrections into account, one might be tempted to rescale our NLO result for the off-shell cross section by using the relative impact of the QCD corrections beyond NLO evaluated in the off-shell region for the signal contribution [92]. Needless to say, much care should be taken when following such approach.

In this Letter, we have studied the production of four charged leptons in pp collisions at 13 TeV, and we have computed the NLO QCD corrections to the loop-induced gluon fusion contribution. Our computation consistently accounts for the Higgs boson signal, its corresponding background and their interference. The contribution from heavy-quark loops is exactly included in the calculation except for the two-loop $gg \rightarrow ZZ \rightarrow 4\ell$ diagrams, for which the heavy-quark effects are approximated through a reweighting procedure. Our calculation is combined with the NNLO QCD and NLO EW corrections in the quark-annihilation channel, and it includes all partonic channels, spin correlations and off-shell effects. The computation is implemented in the MATRIX framework and allows us to separately study the Higgs boson signal, the background and the interference contributions. Those are the central theoretical ingredients of experimental analyses that place bounds on the total Higgs boson width. In particular, for the background and the interference our calculation constitutes the most advanced prediction. We look forward to applications of this calculation and the corresponding implementation in MATRIX to off-shell Higgs boson studies at the LHC and beyond.

Acknowledgements. We thank Fabrizio Caola and Raoul Röntsch for discussions and for providing details on their computations and results. We would also like to express our gratitude to Jean-Nicholas Lang, Jonas Lindert and Federico Buccioni for providing private amplitudes and clarifications. This work is supported in part by the Swiss National Science Foundation (SNF) under contract 200020_188464. The work of JY is supported by Forschungskredit der Universität Zürich, Verfügung Nr. [FK-19-092], and that of SK by the ERC Starting Grant 714788 REINVENT.

References

- [1] G. Aad et al. (ATLAS), *Phys. Lett.* **B716**, 1 (2012), [arXiv:1207.7214 \[hep-ex\]](#).
- [2] S. Chatrchyan et al. (CMS), *Phys. Lett. B* **716**, 30 (2012), [arXiv:1207.7235 \[hep-ex\]](#).
- [3] N. Kauer and G. Passarino, *JHEP* **1208**, 116 (2012), [arXiv:1206.4803 \[hep-ph\]](#).
- [4] F. Caola and K. Melnikov, *Phys. Rev.* **D88**, 054024 (2013), [arXiv:1307.4935 \[hep-ph\]](#).

- [5] J. M. Campbell, R. K. Ellis and C. Williams, *JHEP* **04**, 060 (2014), arXiv:1311.3589 [hep-ph].
- [6] J. M. Campbell, R. K. Ellis and C. Williams, *Phys. Rev.* **D89**, 053011 (2014), arXiv:1312.1628 [hep-ph].
- [7] J. M. Campbell, R. K. Ellis and C. Williams, *PoS* **LL2014**, 008 (2014), arXiv:1408.1723 [hep-ph].
- [8] V. Khachatryan *et al.* (CMS), *Phys. Lett. B* **736**, 64 (2014), arXiv:1405.3455 [hep-ex].
- [9] G. Aad *et al.* (ATLAS), *Eur. Phys. J.* **C75**, 335 (2015), arXiv:1503.01060 [hep-ex].
- [10] V. Khachatryan *et al.* (CMS), *Phys. Rev. D* **92**, 072010 (2015), arXiv:1507.06656 [hep-ex].
- [11] V. Khachatryan *et al.* (CMS), *JHEP* **09**, 051 (2016), arXiv:1605.02329 [hep-ex].
- [12] M. Aaboud *et al.* (ATLAS), *Phys. Lett.* **B786**, 223 (2018), arXiv:1808.01191 [hep-ex].
- [13] A. M. Sirunyan *et al.* (CMS), *Phys. Rev. D* **99**, 112003 (2019), arXiv:1901.00174 [hep-ex].
- [14] B. Mele, P. Nason and G. Ridolfi, *Nucl. Phys.* **B357**, 409 (1991).
- [15] J. Ohnemus and J. Owens, *Phys. Rev.* **D43**, 3626 (1991).
- [16] J. Ohnemus, *Phys. Rev.* **D50**, 1931 (1994), hep-ph/9403331.
- [17] L. J. Dixon, Z. Kunszt and A. Signer, *Phys. Rev.* **D60**, 114037 (1999), hep-ph/9907305.
- [18] J. M. Campbell and R. K. Ellis, *Phys. Rev.* **D60**, 113006 (1999), hep-ph/9905386.
- [19] L. J. Dixon, Z. Kunszt and A. Signer, *Nucl. Phys.* **B531**, 3 (1998), hep-ph/9803250.
- [20] E. Accomando, A. Denner and A. Kaiser, *Nucl. Phys.* **B706**, 325 (2005), hep-ph/0409247.
- [21] A. Bierweiler, T. Kasprzik and J. H. Kühn, *JHEP* **1312**, 071 (2013), arXiv:1305.5402 [hep-ph].
- [22] J. Baglio, L. D. Ninh and M. M. Weber, *Phys. Rev.* **D88**, 113005 (2013), arXiv:1307.4331 [hep-ph].
- [23] B. Biedermann, A. Denner, S. Dittmaier, L. Hofer and B. Jäger, *Phys. Rev. Lett.* **116**, 161803 (2016), arXiv:1601.07787 [hep-ph].
- [24] B. Biedermann, A. Denner, S. Dittmaier, L. Hofer and B. Jäger, *JHEP* **01**, 033 (2017), arXiv:1611.05338 [hep-ph].
- [25] S. Kallweit, J. M. Lindert, S. Pozzorini and M. Schönherr, *JHEP* **11**, 120 (2017), arXiv:1705.00598 [hep-ph].
- [26] M. Chiesa, A. Denner and J.-N. Lang, *Eur. Phys. J.* **C78**, 467 (2018), arXiv:1804.01477 [hep-ph].
- [27] J. van der Bij and E. N. Glover, *Phys. Lett.* **B206**, 701 (1988).
- [28] D. A. Dicus, C. Kao and W. W. Repko, *Phys. Rev.* **D36**, 1570 (1987).

- [29] T. Matsuura and J. van der Bij, *Z. Phys.* **C51**, 259 (1991).
- [30] C. Zecher, T. Matsuura and J. van der Bij, *Z. Phys.* **C64**, 219 (1994), [hep-ph/9404295](#).
- [31] T. Binoth, N. Kauer and P. Mertsch, *Proceedings DIS 2008*, 142 (2008), [arXiv:0807.0024 \[hep-ph\]](#).
- [32] J. M. Campbell, R. K. Ellis and C. Williams, *JHEP* **1110**, 005 (2011), [arXiv:1107.5569 \[hep-ph\]](#).
- [33] N. Kauer, *JHEP* **12**, 082 (2013), [arXiv:1310.7011 \[hep-ph\]](#).
- [34] F. Cascioli, S. Höche, F. Krauss, P. Maierhöfer, S. Pozzorini and F. Siegert, *JHEP* **1401**, 046 (2014), [arXiv:1309.0500 \[hep-ph\]](#).
- [35] N. Kauer, C. O'Brien and E. Vryonidou, *JHEP* **10**, 074 (2015), [arXiv:1506.01694 \[hep-ph\]](#).
- [36] F. Caola, K. Melnikov, R. Röntsch and L. Tancredi, *Phys. Rev.* **D92**, 094028 (2015), [arXiv:1509.06734 \[hep-ph\]](#).
- [37] F. Caola, M. Dowling, K. Melnikov, R. Röntsch and L. Tancredi, *JHEP* **07**, 087 (2016), [arXiv:1605.04610 \[hep-ph\]](#).
- [38] S. Alioli, F. Caola, G. Luisoni and R. Röntsch, *Phys. Rev.* **D95**, 034042 (2017), [arXiv:1609.09719 \[hep-ph\]](#).
- [39] F. Caola, J. M. Henn, K. Melnikov, A. V. Smirnov and V. A. Smirnov, *JHEP* **1506**, 129 (2015), [arXiv:1503.08759 \[hep-ph\]](#).
- [40] A. von Manteuffel and L. Tancredi, *JHEP* **1506**, 197 (2015), [arXiv:1503.08835 \[hep-ph\]](#).
- [41] M. Grazzini, S. Kallweit, M. Wiesemann and J. Y. Yook, *JHEP* **03**, 070 (2019), [arXiv:1811.09593 \[hep-ph\]](#).
- [42] J. M. Campbell, R. K. Ellis, M. Czakon and S. Kirchner, *JHEP* **08**, 011 (2016), [arXiv:1605.01380 \[hep-ph\]](#).
- [43] F. Cascioli, T. Gehrmann, M. Grazzini, S. Kallweit, P. Maierhöfer, A. von Manteuffel, S. Pozzorini, D. Rathlev, L. Tancredi and E. Weihs, *Phys. Lett.* **B735**, 311 (2014), [arXiv:1405.2219 \[hep-ph\]](#).
- [44] G. Heinrich, S. Jahn, S. P. Jones, M. Kerner and J. Pires, *JHEP* **03**, 142 (2018), [arXiv:1710.06294 \[hep-ph\]](#).
- [45] M. Grazzini, S. Kallweit and D. Rathlev, *Phys. Lett.* **B750**, 407 (2015), [arXiv:1507.06257 \[hep-ph\]](#).
- [46] S. Kallweit and M. Wiesemann, *Phys. Lett.* **B786**, 382 (2018), [arXiv:1806.05941 \[hep-ph\]](#).
- [47] T. Gehrmann, A. von Manteuffel, L. Tancredi and E. Weihs, *JHEP* **1406**, 032 (2014), [arXiv:1404.4853 \[hep-ph\]](#).
- [48] F. Caola, J. M. Henn, K. Melnikov, A. V. Smirnov and V. A. Smirnov, *JHEP* **1411**, 041 (2014), [arXiv:1408.6409 \[hep-ph\]](#).

- [49] T. Gehrmann, A. von Manteuffel and L. Tancredi, *JHEP* **09**, 128 (2015), [arXiv:1503.04812 \[hep-ph\]](#).
- [50] M. Grazzini, S. Kallweit, J. M. Lindert, S. Pozzorini and M. Wiesemann, *JHEP* **02**, 087 (2020), [arXiv:1912.00068 \[hep-ph\]](#).
- [51] M. Grazzini, S. Kallweit and M. Wiesemann, *Eur. Phys. J.* **C78**, 537 (2018), [arXiv:1711.06631 \[hep-ph\]](#).
- [52] F. Cascioli, P. Maierhöfer and S. Pozzorini, *Phys. Rev. Lett.* **108**, 111601 (2012), [arXiv:1111.5206 \[hep-ph\]](#).
- [53] F. Buccioni, S. Pozzorini and M. Zoller, *Eur. Phys. J.* **C78**, 70 (2018), [arXiv:1710.11452 \[hep-ph\]](#).
- [54] F. Buccioni, J.-N. Lang, J. M. Lindert, P. Maierhöfer, S. Pozzorini, H. Zhang and M. F. Zoller, *Eur. Phys. J.* **C79**, 866 (2019), [arXiv:1907.13071 \[hep-ph\]](#).
- [55] M. Grazzini, S. Kallweit, M. Wiesemann and J. Y. Yook, *Phys. Lett. B* **804**, 135399 (2020), [arXiv:2002.01877 \[hep-ph\]](#).
- [56] M. Aaboud et al. (ATLAS), *JHEP* **04**, 048 (2019), [arXiv:1902.05892 \[hep-ex\]](#).
- [57] B. Agarwal, S. P. Jones and A. von Manteuffel, (2020), [arXiv:2011.15113 \[hep-ph\]](#).
- [58] C. Brønnum-Hansen and C.-Y. Wang, (2021), [arXiv:2101.12095 \[hep-ph\]](#).
- [59] S. Catani, L. Cieri, D. de Florian, G. Ferrera and M. Grazzini, *Nucl. Phys.* **B881**, 414 (2014), [arXiv:1311.1654 \[hep-ph\]](#).
- [60] M. Spira, A. Djouadi, D. Graudenz and P. M. Zerwas, *Nucl. Phys. B* **453**, 17 (1995), [arXiv:hep-ph/9504378](#).
- [61] C. Anastasiou, S. Beerli, S. Bucherer, A. Daleo and Z. Kunszt, *JHEP* **01**, 082 (2007), [arXiv:hep-ph/0611236](#).
- [62] R. Harlander and P. Kant, *JHEP* **12**, 015 (2005), [arXiv:hep-ph/0509189](#).
- [63] U. Aglietti, R. Bonciani, G. Degrossi and A. Vicini, *JHEP* **01**, 021 (2007), [arXiv:hep-ph/0611266](#).
- [64] R. V. Harlander, M. Prausa and J. Usovitsch, *JHEP* **10**, 148 (2019), [Erratum: *JHEP* 08, 101 (2020)], [arXiv:1907.06957 \[hep-ph\]](#).
- [65] M. Grazzini, S. Kallweit, D. Rathlev and A. Torre, *Phys. Lett.* **B731**, 204 (2014), [arXiv:1309.7000 \[hep-ph\]](#).
- [66] M. Grazzini, S. Kallweit and D. Rathlev, *JHEP* **07**, 085 (2015), [arXiv:1504.01330 \[hep-ph\]](#).
- [67] T. Gehrmann, M. Grazzini, S. Kallweit, P. Maierhöfer, A. von Manteuffel, S. Pozzorini, D. Rathlev and L. Tancredi, *Phys. Rev. Lett.* **113**, 212001 (2014), [arXiv:1408.5243 \[hep-ph\]](#).
- [68] M. Grazzini, S. Kallweit, S. Pozzorini, D. Rathlev and M. Wiesemann, *JHEP* **08**, 140 (2016), [arXiv:1605.02716 \[hep-ph\]](#).

- [69] M. Grazzini, S. Kallweit, D. Rathlev and M. Wiesemann, *Phys. Lett.* **B761**, 179 (2016), [arXiv:1604.08576 \[hep-ph\]](#).
- [70] M. Grazzini, S. Kallweit, D. Rathlev and M. Wiesemann, *JHEP* **05**, 139 (2017), [arXiv:1703.09065 \[hep-ph\]](#).
- [71] S. Kallweit, V. Sotnikov and M. Wiesemann, (2020), [arXiv:2010.04681 \[hep-ph\]](#).
- [72] M. Grazzini, S. Kallweit, D. Rathlev and M. Wiesemann, *JHEP* **08**, 154 (2015), [arXiv:1507.02565 \[hep-ph\]](#).
- [73] S. Kallweit, E. Re, L. Rottoli and M. Wiesemann, (2020), [arXiv:2004.07720 \[hep-ph\]](#).
- [74] M. Wiesemann, L. Rottoli and P. Torrielli, *Phys. Lett. B* **809**, 135718 (2020), [arXiv:2006.09338 \[hep-ph\]](#).
- [75] E. Re, M. Wiesemann and G. Zanderighi, [arXiv:1805.09857 \[hep-ph\]](#).
- [76] P. F. Monni, P. Nason, E. Re, M. Wiesemann and G. Zanderighi, *JHEP* **05**, 143 (2020), [arXiv:1908.06987 \[hep-ph\]](#).
- [77] S. Alioli, A. Broggio, S. Kallweit, M. A. Lim and L. Rottoli, *Phys. Rev. D* **100**, 096016 (2019), [arXiv:1909.02026 \[hep-ph\]](#).
- [78] P. F. Monni, E. Re and M. Wiesemann, *Eur. Phys. J. C* **80**, 1075 (2020), [arXiv:2006.04133 \[hep-ph\]](#).
- [79] D. Lombardi, M. Wiesemann and G. Zanderighi, (2020), [arXiv:2010.10478 \[hep-ph\]](#).
- [80] MUNICH is the abbreviation of “MULTI-chaNNel Integrator at Swiss (CH) precision”—an automated parton level NLO generator by S. Kallweit. In preparation.
- [81] S. Catani and M. Seymour, *Phys. Lett.* **B378**, 287 (1996), [hep-ph/9602277](#).
- [82] S. Catani and M. Seymour, *Nucl. Phys.* **B485**, 291 (1997), [hep-ph/9605323](#).
- [83] S. Catani and M. Grazzini, *Phys. Rev. Lett.* **98**, 222002 (2007), [hep-ph/0703012](#).
- [84] S. Actis, A. Denner, L. Hofer, J.-N. Lang, A. Scharf and S. Uccirati, *Comput. Phys. Commun.* **214**, 140 (2017), [arXiv:1605.01090 \[hep-ph\]](#).
- [85] A. Denner, J.-N. Lang and S. Uccirati, *Comput. Phys. Commun.* **224**, 346 (2018), [arXiv:1711.07388 \[hep-ph\]](#).
- [86] The VVAMP project, by T. Gehrmann, A. von Manteuffel, and L. Tancredi, is publicly available at <http://vvamp.hepforge.org>.
- [87] J. M. Campbell, R. K. Ellis and C. Williams, *JHEP* **1107**, 018 (2011), [arXiv:1105.0020 \[hep-ph\]](#).
- [88] J. M. Campbell, R. K. Ellis and W. T. Giele, *Eur. Phys. J. C* **75**, 246 (2015), [arXiv:1503.06182 \[physics.comp-ph\]](#).

- [89] A. Denner, S. Dittmaier, M. Roth and L. H. Wieders, *Nucl. Phys.* **B724**, 247 (2005), [Erratum: *Nucl. Phys.* B854, 504 (2012)], [hep-ph/0505042](#).
- [90] C. Patrignani *et al.* (Particle Data Group), *Chin. Phys.* **C40**, 100001 (2016).
- [91] V. Bertone, S. Carrazza, N. P. Hartland and J. Rojo (NNPDF), *SciPost Phys.* **5**, 008 (2018), [arXiv:1712.07053 \[hep-ph\]](#).
- [92] C. Anastasiou, C. Duhr, F. Dulat, E. Furlan, T. Gehrmann, F. Herzog, A. Lazopoulos and B. Mistlberger, *JHEP* **05**, 058 (2016), [arXiv:1602.00695 \[hep-ph\]](#).
- [93] J. R. Andersen *et al.* (LHC Higgs Cross Section Working Group), (2013), [10.5170/CERN-2013-004](#), [arXiv:1307.1347 \[hep-ph\]](#).
- [94] G. Passarino, *Eur. Phys. J. C* **74**, 2866 (2014), [arXiv:1312.2397 \[hep-ph\]](#).